Graded Index Chalcogenide Fibers with Nanostructured Core

Meneghetti, Marcello; Forestier, Xavier; Petersen, Christian Rosenberg; Kasztelanic, Rafał; Klimczak, Mariusz; Bang, Ole; Buczyński, Ryszard; Troles, Johann

Published in:
Advanced Photonics Research

Link to article, DOI:
10.1002/adpr.202000091

Publication date:
2021

Document Version
Peer reviewed version

Graded Index Chalcogenide Fibers with Nanostructured Core

*Marcello Meneghetti Xavier Forestier Christian R. Petersen Rafa l Kasztelanic Mariusz Klimczak Ole Bang Ryszard Buczyński Johann Troles**

Dr. Marcello Meneghetti, Prof. Johann Troles
Univ Rennes, CNRS, ISCR - UMR 6226 F-35000 Rennes, France
Email Address: johann.troles@univ-rennes1.fr
Dr. Marcello Meneghetti, Dr. Christian R. Petersen, Prof. Ole Bang
DTU Fotonik, Department of Photonics Engineering, Technical University of Denmark, DK-2800 Kgs. Lyngby, Denmark
Prof. Ole Bang
NORBLIS Ivs, Virumgade 35D, 2830 Virum
Xavier Forestier, Dr. Rafał, Kasztelanic, Prof. Ryszard Buczyński
Institute of Electronic Materials Technology, Wolczynska 133, 01-919 Warsaw, Poland
Xavier Forestier, Dr. Rafał, Kasztelanic, Dr. Mariusz Klimczak, Prof. Ryszard Buczyński
University of Warsaw, Faculty of Physics, Pasteura 7, 02-093 Warsaw, Poland

Keywords: *Graded index fibers, Chalcogenide glasses, Infrared optics, Supercontinuum*

Fabrication of graded index (GRIN) fibers was for a long time limited to ion-exchange, modified chemical vapour deposition (MCVD) or other deposition techniques. Recently, the nanostructuring of an all-solid core in fibers has proven to be a versatile and low cost alternative for the production of gradient index optical fibers. In this work, high purity chalcogenide glasses in the Ge-As-Se glass system, synthesized in-house, were used for stacking and drawing chalcogenide nanostructured GRIN fibers designed using the Maxwell-Garnett effective medium theory, simulated annealing and genetic algorithms. The successful generation of a supercontinuum spanning the mid-infrared from 3 μm to 6 μm, pumping at a central wavelength of 4 μm using an Optical Parametric Oscillator with femtoseconds pulses, is also reported.

In the last twenty years the field of chalcogenide glasses has seen increasing interest, thanks to their strong nonlinearity and broadband transparency in the mid-infrared part of the spectrum. In particular, chalcogenide fibers, having broad transmission windows in the $1-12\ \mu$m range [1], can be especially suitable for nonlinear optical switching in telecommunications, molecular sensing, imaging and spectroscopy [2, 3] and can form the basis of supercontinuum broadband lasers with a brightness orders of magnitude higher than synchrotrons [4]. Furthermore, chalcogenides exhibit some of the highest nonlinear refractive indices among known glasses, allowing for the observation of nonlinear optical effects in very short segments of fiber [5-8]. In the field of nonlinear optics, graded-index (GRIN) fibers are generating a strong interest for the study of complex multimode beam dynamics [9-12], as they enable simultaneous tunability of chromatic and intermodal dispersion. Despite the strong interest, there is no reported example of a GRIN

chalcogenide glass fiber. This is due to the lack of a suitable technique for their development. While chemical vapor deposition (CVD) has successfully been employed for silica GRIN fibers, it is currently incompatible with chalcogenides. Recently, a more versatile technique for producing optical elements with arbitrarily shaped refractive index (RI) profiles has been introduced [13], based on the stack-and-draw process. It involves the design of a 2D binary pattern of sub-wavelength elements using two materials with different RI. The result is an effective medium whose RI at every point is the local spatial average of the two materials. The RI profile is therefore dependent on the pattern arrangement. This fabrication method has already been demonstrated to be suitable for the production of silica and borosilicate GRIN optical fibers [14, 15]. Owing to the intrinsic versatility of this pattern-based RI profile design, which does not share with deposition techniques the necessity to maintain a circular symmetry, other applications such as the fabrication of multi-core and polarization maintaining fibers have been demonstrated [16, 17]. In 2017, chalcogenide GRIN fibers produced by the stack and draw technique were investigated numerically [18], showing in theory the possibility of a high degree of chromatic dispersion control and the feasibility of obtaining flat, all normal dispersion profiles over a large portion of the mid-infrared spectral range. The latter property is of high interest for obtaining significant improvements in some applications of supercontinuum generation (SCG) [19], such as optical coherence tomography [20, 21], multi-spectral imaging [22], ultrashort pulse generation [23], and communications[24]. Moreover, the development of all-solid GRIN fibers could represent a valid alternative to the consolidated photonic crystal fibers (PCFs) approach for the management of dispersion and modal properties in chalcogenide fibers. Indeed, for this family of glasses, the photonic crystal cladding is usually limited to maximum three rings of air holes due to fabrication limits in preform development and control of the fiber drawing process [25-27], and the robustness of chalcogenide PCFs is also limited due to glass degradation processes related to the penetration of water vapor in the air holes[28]. In this work, high purity germanium arsenic selenide glasses have been used to develop the first chalcogenide GRIN fiber, to show the suitability of nanostructurization by the stack and draw technique as a platform to fabricate chalcogenide fibers with a large variety of RI profiles. In addition, SCG was demonstrated in the fabricated fiber as a proof-of-concept experiment to validate the proposed fabrication approach.

For the realization of the fiber, two compositions of glass in the Ge-As-Se ternary system have been selected and developed: $Ge_5As_{30}Se_{65}$ and $Ge_{10}As_{22}Se_{68}$. These glasses were chosen based on their increased resistance to crystallization and degradation during multiple heating steps, given by the addition of Ge to selenide glasses [29]. The glasses have a difference in T_g of only 10 and similar viscosity profiles, allowing for simultaneous drawing. These compositions also exhibit a significant RI difference ($\Delta n \simeq 0.1$, as visible in Figure 1.a), allowing for a high contrast RI profile in the fiber's core. The glasses were prepared using a double distillation process [30], resulting in an attenuation baseline ≤ 0.1 dB/m and in general losses below 1 dB/m between 2 and 9 μm, apart from the Se-H impurity band around 4.5 μm (Figure 1.b). From these glasses, rods with a diameter of $450\,\mu$m were produced. Subsequently, a proper stack configuration for the core of the fiber, shown in Figure 1.d, was designed using an in-house developed software based on the simulated annealing[13], genetic algorithms and random walk model. A parabolic profile of the RI was chosen for the core, as this would enable us to draw an analogy to the most common RI profile of the mature silica glass GRIN fibers. The number of elements to be used in the design of the pattern, namely 817 (33 elements on the diagonal, with a diameter of 330 nm each for a target core size of 10 μm), was decided as a compromise between different factors: the

accuracy in reproducing the desired profile, the necessity for the size of the individual elements in the core to be subwavelength, the fact that by decreasing the rods diameter they lose rigidity and it becomes more difficult to manually stack the pattern, and the fact that in the furnaces used for the drawing of canes there is a limit to the size of preforms that can be heated uniformly. The rods were stacked according to the designed pattern, and the stacks were drawn into compact GRIN canes to be used as cores for a classical rod-in-tube fiber drawing (Figure 1.c,e,f). The cladding tubes were produced by rotational casting, using the same low-index glass composition as in the rods. Once the tubes and core canes were prepared, a standard rod-in-tube technique was used to draw the final fibers, with an external diameter of 125 μm and a core diameter of 10 μm. Fiber variants with core diameters of 4.4, 5.6, 7, 20 and 40 μm were also drawn to study the influence of the core diameter on the light propagation properties. While the fibers with large core diameters were directly drawn, the ones with core diameter smaller than 10 μm were obtained by a tapering process, and cut at the transition points in order to have samples with uniform diameters. Both optical (Figure 2.a,b,c) and electron microscopy images have shown an almost perfect collapsing of the structure, with only very few instances of defects in the form of small holes among a large number of analyzed samples. Despite the numerous thermal steps in the production process, no signs of crystallization were found. Measurements performed by energy dispersive X-Ray spectroscopy (EDS) along the diameter of the fibers show a compositional variation compatible with the desired RI profile (Figure 2.d). However, the optical losses measured for the 10 μm core fiber are two orders of magnitude larger than the ones of the starting materials (Figure 2.e). The absence of crystals or visible defects at the interfaces between the rods suggests that this excess of losses could be related to the interaction between the light and the core's structure itself, leading to scattering or diffraction caused by the elements of different RI. This, if true, would cause the attenuation to be strongly dependent on the size of the elements and to be more pronounced at shorter wavelengths. Indeed all the fibers obtained by tapering performed better than the original fiber in terms of optical losses in the measured range, with a difference of more than 20 dB/m, as visible in Figure 2.f. Furthermore, the attenuation curves presented in Figure 2.f show that the optical losses are strongly dependent on both core size and wavelength. As an example, the optical losses of the 10 μm core fiber reach more than 120 dB/m at 1.2 μm and decrease until 70 dB/m at 2.2 μm. For the fibers with smaller cores, even if the curves are very noisy, it can be noticed that the optical losses decrease with the core size. In this wavelength window a minimum of attenuation, corresponding to a wavelength of 1.98 μm, has been recorded to be close to 25 dB/m in the fiber with the smallest core (4.4 μm of diameter). On the other hand, in the mid-IR there was no significant decrease in transmission going from the 7 μm core to the 10 μm core fiber, while a dramatic increase in losses was found going from the 10 μm to the 20 μm core: despite the larger core, the output power while attempting SCG was found to be only of 1.7 mW for the 20 μm core fiber, as opposed to 30 mW for the 10 μm core fiber. These results seem to confirm a correlation between the transmission loss, and the size of the individual core elements relative to the wavelength. Even if no evidence about the presence of crystals or defects in the fiber cores has been observed, it can't be totally excluded that additional losses may be induced by small interface defect [31]. In this case, the reported increase in optical losses could be the sum of the effects of light scattering due to the structure of the fiber core and to interface defects. While such losses could be detrimental to applications in the near-IR, they could also be exploited as a unique method for achieving all-fiber long-pass filtering for mid-IR applications. The dispersion of the GRIN fibers was evaluated both by measurements and simulations. The dispersion of the

fundamental mode was simulated over the entire transparency range, starting from the core pattern configuration and using a finite difference method (FDE). The calculations were performed for the core diameters in which SCG was achieved and, in addition, for diameters of 20 and 40 μm, in order to evaluate the dependence of dispersion on the size of the core. The resulting dispersion curves are presented in Figure 3.a. It can be noticed that the two fibers with larger core size have their zero dispersion wavelength (ZDW) at around 7 μm, which is close to the material ZDW of the glasses [32]. Reducing the core size results in a strong deviation from the material dispersion, with both simulated fibers having an all-normal dispersion (ANDi) profile over the whole transparency window (see Figure 3.a). More specifically, the 10 μm core fiber has an extremely flat dispersion profile ranging between -10 and -20 $ps/nm \cdot km$ from 4.5 μm to 11 μm, while the 7 and 5.6 μm core ones exhibits stronger normal dispersion and a saddle-like shape (see Figure 3.a). For applications in high coherence SCG, where a flat and near-zero normal dispersion is of great importance, a value of around 10 μm for the core diameter seems to be ideal. Nonetheless, the definite change of behavior visible when further reducing the core diameter is an indicator of the great versatility of the presented fabrication technique in tailoring the dispersion profile by choosing appropriate design of the core pattern and diameter. In order to confirm the dispersion values and dispersion behavior of the fibers, experimental measurements were performed in both the near-IR and mid-IR on the fiber with a core size of 10 μm (see Figure 3.b). In the near infrared the measured dispersion values are in agreement with the computed values from 1.2 μm to 2 μm (Figure 3.b, blue line), while a mismatch is observed from 2 to 2.4 μm, probably due to experimental errors. In the mid infrared, instead, the agreement between calculated and measured values appears to be good over the whole measurement range (between 3.4 and 4.5 μm). These results confirm the dispersion behaviors simulated in the chalcogenide grin fiber. Lastly, to demonstrate the applicability of GRIN chalcogenide fibers for nonlinear applications, the 5.6 μm, 7 μm, and 10 μm core fibers were tested for ANDi SCG. Figure 3.c shows the output spectrum of the three fibers, corresponding to an average output power of 10.5 mW, 22 mW, and 30 mW, respectively. Despite the higher transmission of the 10 μm core fiber, the 7 μm core fiber was found to produce the broadest spectrum spanning from $< 2.6 - 6 \mu m$. This was attributed to the higher nonlinear coefficient of a fiber with smaller core combined with a flatter dispersion profile near the 4 μm pump wavelength. While the 10 μm core fiber has a lower numerical value of dispersion, the dispersion slope is higher and more importantly the value of the dispersion is continuously increasing up to a wavelength of about 6.5 μm, while the dispersion varies only 6.31 $ps/nm \cdot km$ between 4.08-10.48 μm in the 7 μm core simulated fiber. The observed spectral broadening dynamics with increased pump power is illustrated in Figure 3.d for the 7 μm core fiber. The figure shows the smooth, symmetric broadening typically associated with self-phase modulation and optical wave breaking of femtosecond ANDi SCG dynamics[33]. The output beam was also imaged to confirm confinement of the light to the core of the fiber, as shown in Figure 3.e. It is known from previous studies in silica PCFs that such an ANDi continuum can be highly coherent, provided that the noise of the pump laser is fairly low [34], and the product of the nonlinearity, peak power, and fiber length is maintained at a moderate level [35]. The pump relative intensity noise was measured to be 2.1%, and from the 22 mW average output power the peak power coupled to the fiber was estimated to be around 16.5 kW, taking into consideration the Fresnel reflection at the output facet (22.6% for n=2.67), and 30 dB/m propagation loss (6.6 dB for 22 cm fiber length). Given the complex spatio-temporal nature

of SCG in GRIN fibers [12, 36] it is difficult to predict whether coherence is preserved at these conditions, but judging from the output spectrum with increasing pump power there is no indication of modal or geometric instabilities. The fiber's output was imaged to confirm the confinement of light in the fiber's core, as shown in Figure 3.e.

In summary, the first implementation of a chalcogenide graded index fiber has been demonstrated, with a nanostructured core composed of nanorods of two different refractive indices. Such a fiber could allow for an upscaling of the average power injected in chalcogenide fibers by achieving confinement in large cores with low intermodal dispersion, and, thanks to the high nonlinear refractive index of selenide glasses, be an ideal platform for the study of intermodal nonlinearities, such as beam self-cleaning instabilities and Raman scattering. Despite the high losses, light transmission was achieved in the fiber both in the near- and mid- infrared. The correlation highlighted between the level of losses and the size of the elements composing the core pattern shows a possibility to achieve an optical fiber with improved optical properties in the future using the technological platform demonstrated in scope of this work, which is presently the sole reported one allowing to obtain graded index profiles in chalcogenide fiber. According to the simulations performed, this method to produce fibers enables a high versatility in the management of dispersion, notably with the possibility to have an ultra-flat ANDi profile over the whole mid-IR spectral region. For our next studies, manhours used to manually stack the GRIN preform could be reduced by the use of a robotic assembly. Moreover, this method allows the development of fibers with arbitrary refractive index distribution in the core. All considered nanostructured fibers are all-solid, therefore their integration with other fibers in cascaded systems as well as robustness and ease of operation (cutting, fusion splicing, integration) is similar to standard step-index chalcogenide fibers and it allows one to avoid all issues related to handling air-glass photonic crystal fibers. In addition, a broadband supercontinuum spectrum spreading from 2 to 6 μm has been obtained by pumping this innovative fiber at a wavelength of 4 μm .

Experimental Section

Core pattern design

With a continuous GRIN parabolic profile as a target, the binary pattern of rods to be used has been determined by a simulated annealing genetic algorithm. As a starting point for the calculation, an initial distribution of the two types of rods with different refractive index can be determined either randomly or by using different halftoning algorithms [37]. The effective refractive index profile of the structure is then calculated based on the Maxwell Garnett mixing formula [38], and the difference between it and the target refractive index profile is defined as a cost function for the simulated annealing algorithm used to optimize the structure. [39] In every iteration the refractive index of a randomly selected rod is changed to its other possible value, and the cost function is recalculated. The process is repeated until the cost function cannot be reduced anymore. This algorithm is effective and allows one to obtain a binary pattern that mimics a continuous refractive index distribution, although it is time consuming and the final result strongly depends on the initial rod distribution. As a solution to the last problem, further structure optimization is carried on with support of genetic algorithm methods, processing in parallel several patterns. In every iteration step, called 'generation', the different structures exchange part of their patterns to generate random changes. In this way a large set of diverse patterns is considered, local minima of cost function are avoided and finally a pattern better matching the

target continuous refractive index distribution is obtained. As a final verification light propagation in the obtained binary nanostructured pattern is compared with the one in the ideal target continuous refractive index profile using a full-vector beam propagation method. Similar performance confirms the correctness of the nanostructured binary pattern.

Imaging

All the fibers drawn were cleaved in a large number of different points and imaged using a Keyence VHX 5000 digital optical microscope, in order to check for the presence of defects. On some of the cleaves, energy dispersive spectroscopy (EDS) was used to verify the distributions of the chemical elements composing the fiber along its diameter.

Attenuation measurements

As a first mean to verify light transmission in the three fibers initially obtained (10, 20 and 40 μm cores), they were injected with light from a 1.55 μm CW laser, and their output field was imaged using a microscope objective coupled with a CCD camera. Graphite dissolved in alcohol was applied on the outer surface of the fibers near the injection point to remove light injected in the cladding. The attenuation in the mid infrared of the 10 μm core fiber was measured with a standard cutback technique using a Bruker T37 Fourier Transform Infrared (FTIR) spectroscopy apparatus and an external MCT detector to collect the signal. Due to the very low transmittance observed, only a single cutback with a length of about 10 cm was performed. No attenuation measurements could be performed with the FTIR (in the 2-11 μm mid-IR region) in the fibers with different core sizes, because of either the small amount of light coupled in the core (fibers with core diameter $\leq$ 7 μm) or because of the high optical losses (fibers with core diameter $\geq$ 20 μm). In order to get more reliable information on the attenuation at short wavelengths, a second measurement was performed. For this, light from a supercontinuum source with a spectral range spanning from 200 to 2400 nm (LEUKOS, France) was injected in the fiber, and a Yokogawa AQ6375B optical spectrum analyzer operating in the wavelength range between 1200 and 2400 nm, was used to detect the signal. The light with wavelengths shorter than 1.2 μm was filtered out from the output of the supercontinuum source in order to avoid absorption-related damage to the fiber. Two attenuation curves were collected, from two cutbacks of $\sim$ 5 cm each, and their average was taken.

Dispersion measurements

The NIR dispersion measurements were performed using a Mach-Zehnder interferometer [40]. For the calculation of $n(\lambda)$, the small OPD induced by the optical elements in the setup was also taken into consideration. This was done by applying a correction to the raw data, derived from the dispersion characteristics and thicknesses of the lenses and filters used. The group RI was then fitted to a 5-term power series[41]:

$$n(\lambda) = \frac{A_1}{\lambda^4} + \frac{A_2}{\lambda^2} + A_3 + A_4\lambda^2 + A_5\lambda^4$$

The MIR dispersion measurements were performed using a custom NKT SuperK MIR supercontinuum source and a balanced Mach-Zehnder interferometer. The combined interference signal from the fiber and reference arms was coupled to an InF_3 single-mode fiber and analyzed using a scanning spectrometer. Finally, the dispersion was derived from fitting the position of the interference fringes with respect to wavelength to a modified Cauchy equation for the effective

refractive index.

Supercontinuum generation

ANDi SCG was achieved using a 4 μm wavelength 250 fs pump based on optical parametric generation [42]. The relative intensity noise of the pump laser was measured by recording the pulse train using a photo detector (100 MHz HgCdTe amplified photovoltaic detector, PDAVJ10 Thorlabs) and a fast oscilloscope (4 GHz,/40 GS/s/10bit, HDO9404 Teledyne Lecroy). The beam was coupled to the fibers using a 4 mm focal length molded aspheric BD-2 lens, and the output was collimated using a similar lens with 1.8 mm focal length. The output power was measured after collimation using a thermal power meter, and the spectrum was analyzed using a silver-halide fiber-coupled Fourier-transform infrared spectrometer.

Supporting Information

Supporting Information is available from the Wiley Online Library or from the author.

Acknowledgements

We acknowledge support from the Horizon 2020 Framework Programme Marie Curie grant No. 722380 [SUPUVIR].

References

[1] J. Troles, V. Shiryaev, M. Churbanov, P. Houizot, L. Brilland, F. Désévédavy, F. Charpentier, T. Pain, G. Snopatin, J.-L. Adam, *Optical Materials* **2009**, *32*, 1 212.

[2] J. Sanghera, I. Aggarwal, *Journal of Non-Crystalline Solids* **1999**, *256* 6.

[3] J. Keirsse, C. Boussard-Plédel, O. Loreal, O. Sire, B. Bureau, B. Turlin, P. Leroyer, J. Lucas, *Journal of Non-Crystalline Solids* **2003**, *326* 430.

[4] C. R. Petersen, P. M. Moselund, L. Huot, L. Hooper, O. Bang, *Infrared Physics & Technology* **2018**, *91* 182.

[5] J. M. Harbold, F. O. Ilday, F. W. Wise, B. G. Aitken, *IEEE Photonics Technology Letters* **2002**, *14*, 6 822.

[6] J. S. Sanghera, L. B. Shaw, P. Pureza, V. Q. Nguyen, D. Gibson, L. Busse, I. D. Aggarwal, C. M. Florea, F. H. Kung, *International Journal of Applied Glass Science* **2010**, *1*, 3 296.

[7] M. Asobe, *Optical Fiber Technology* **1997**, *3*, 2 142.

[8] Q. Coulombier, L. Brilland, P. Houizot, T. Chartier, T. N. N'guyen, F. Smektala, G. Renversez, A. Monteville, D. Méchin, T. Pain, et al., *Optics Express* **2010**, *18*, 9 9107.

[9] G. Lopez-Galmiche, Z. S. Eznaveh, M. Eftekhar, J. A. Lopez, L. Wright, F. Wise, D. Christodoulides, R. A. Correa, *Optics Letters* **2016**, *41*, 11 2553.

[10] L. G. Wright, Z. Liu, D. A. Nolan, M.-J. Li, D. N. Christodoulides, F. W. Wise, *Nature Photonics* **2016**, *10*, 12 771.

[11] U. Teğin, B. Ortaç, *Scientific Reports* **2018**, *8*, 1 1.

[12] M. Eftekhar, Z. Sanjabi-Eznaveh, H. Lopez-Aviles, S. Benis, J. Antonio-Lopez, M. Kolesik, F. Wise, R. Amezcua-Correa, D. Christodoulides, *Nature Communications* **2019**, *10*, 1 1.

[13] F. Hudelist, R. Buczynski, A. Waddie, M. Taghizadeh, *Optics Express* **2009**, *17*, 5 3255.

[14] R. Buczyński, M. Klimczak, T. Stefaniuk, R. Kasztelanic, B. Siwicki, G. Stepniewski, J. Cimek, D. Pysz, R. Stepień, *Optics Express* **2015**, *23*, 20 25588.

[15] X. Forestier, T. Karpate, G. Huss, V. Tombelaine, G. Stepniewski, A. Anuszkiewicz, R. Kasztelanic, A. Filipkowski, D. Pysz, M. Klimczak, et al., *Applied Nanoscience* **2020**, 1–9.

[16] M. Longobucco, J. Cimek, L. Curilla, D. Pysz, R. Buczyński, I. Bugar, In *2018 20th International Conference on Transparent Optical Networks (ICTON)*. IEEE, **2018** 1–4.

[17] D. Michalik, T. Stefaniuk, R. Kasztelanic, R. Buczyński, *JOSA B* **2020**, *37*, 6 1722.

[18] B. Siwicki, A. Filipkowski, R. Kasztelanic, M. Klimczak, R. Buczyński, *Optics Express* **2017**, *25*, 11 12984.

[19] N. Zhang, X. Peng, Y. Wang, S. Dai, Y. Yuan, J. Su, G. Li, P. Zhang, P. Yang, X.

Wang, *Optics Express* **2019**, *27*, 7 10311.

[20] B. Povazay, K. Bizheva, A. Unterhuber, B. Hermann, H. Sattmann, A. Fercher, W. Drexler, A. Apolonski, W. Wadsworth, J. Knight, et al., *Optics Letters* **2002**, *27*, 20 1800.

[21] N. M. Israelsen, C. R. Petersen, A. Barh, D. Jain, M. Jensen, G. Hannesschläger, P. Tidemand-Lichtenberg, C. Pedersen, A. Podoleanu, O. Bang, *Light: Science & Applications* **2019**, *8*, 1 1.

[22] C. R. Petersen, N. Prtljaga, M. Farries, J. Ward, B. Napier, G. R. Lloyd, J. Nallala, N. Stone, O. Bang, *Optics Letters* **2018**, *43*, 5 999.

[23] J. M. Dudley, S. Coen, *Optics Express* **2004**, *12*, 11 2423.

[24] H. Takara, T. Ohara, K. Mori, K. Sato, E. Yamada, Y. Inoue, T. Shibata, M. Abe, T. Morioka, K.-I. Sato, *Electronics Letters* **2000**, *36*, 25 2089.

[25] L. Brilland, F. Smektala, G. Renversez, T. Chartier, J. Troles, T. N. Nguyen, N. Traynor, A. Monteville, *Optics Express* **2006**, *14*, 3 1280.

[26] J. Fatome, C. Fortier, T. N. Nguyen, T. Chartier, F. Smektala, K. Messaad, B. Kibler, S. Pitois, G. Gadret, C. Finot, et al., *Journal of Lightwave Technology* **2009**, *27*, 11 1707.

[27] A. N. Ghosh, M. Meneghetti, C. R. Petersen, O. Bang, L. Brilland, S. Venck, J. Troles, J. M. Dudley, T. Sylvestre, *Journal of Physics: Photonics* **2019**, *1*, 4 044003.

[28] P. Toupin, L. Brilland, D. Mechin, J.-L. Adam, J. Troles, *Journal of Lightwave Technology* **2014**, *32*, 13 2428.

[29] P. Toupin, L. Brilland, J. Trolès, J.-L. Adam, *Optical Materials Express* **2012**, *2*, 10 1359.

[30] M. Meneghetti, C. Caillaud, R. Chahal, E. Galdo, L. Brilland, J.-L. Adam, J. Troles, *Journal of Non-Crystalline Solids* **2019**, *503* 84.

[31] L. Brilland, J. Troles, P. Houizot, F. Desevedavy, Q. Coulombier, G. Renversez, T. Chartier, T. N. Nguyen, J.-L. Adam, N. Traynor, *Journal of the Ceramic Society of Japan* **2008**, *116*, 1358 1024.

[32] H. G. Dantanarayana, N. Abdel-Moneim, Z. Tang, L. Sojka, S. Sujecki, D. Furniss, A. B. Seddon, I. Kubat, O. Bang, T. M. Benson, *Optical Materials Express* **2014**, *4*, 7 1444.

[33] A. M. Heidt, A. Hartung, G. W. Bosman, P. Krok, E. G. Rohwer, H. Schwoerer, H. Bartelt, *Optics Express* **2011**, *19*, 4 3775.

[34] E. Genier, P. Bowen, T. Sylvestre, J. M. Dudley, P. Moselund, O. Bang, *JOSA B* **2019**, *36*, 2 A161.

[35] I. B. Gonzalo, R. D. Engelsholm, M. P. Sørensen, O. Bang, *Scientific Reports* **2018**, *8*, 1 1.

[36] K. Krupa, C. Louot, V. Couderc, M. Fabert, R. Guénard, B. Shalaby, A. Tonello, D. Pagnoux, P. Leproux, A. Bendahmane, et al., *Optics Letters* **2016**, *41*, 24 5785.

[37] P.-M. Jodoin, V. Ostromoukhov, In *Proc. SPIE 5008, Color Imaging VIII: Processing, Hardcopy, and Applications*, *443–454*. **2003** .

[38] A. H. Sihvola, *Electromagnetic mixing formulas and applications*, 47. IET, **1999**.

[39] S. Kirkpatrick, C. D. Gelatt, M. P. Vecchi, *Science* **1983**, *220*, 4598 671.

[40] P. Hlubina, M. Kadulová, D. Ciprian, *Journal of the European Optical Society-Rapid Publications* **2012**, *7*.

[41] P. Hlubina, D. Ciprian, M. H. Frosz, K. Nielsen, In *Proc. SPIE 7389, Optical Measurement Systems for Industrial Inspection VI, 73890J*. **2009** .

[42] C. R. Petersen, R. D. Engelsholm, C. Markos, L. Brilland, C. Caillaud, J. Trolès, O. Bang, *Optics Express* **2017**, *25*, 13 15336.

1 Figures

Figure 1: **a)** Refractive indices of the two glass compositions used, calculated [42] starting from measurements at 1.33 μm and 1.55 μm and from the known refractive index curve of a similar composition [32]. **b)** Attenuation spectra of two of the batches of distilled glass used to prepare the rods, measured by cutback technique with cutback length > 20 m ; the dashed line shows the typical attenuation spectrum of a non distilled Ge-As-Se glass for comparison. **c)** Schematics of the procedure used to develop the chalcogenide GRIN fibers. **d)** Calculated distribution of the high RI (red) and low RI (blue) rods in the stack corresponding to a parabolic refractive index profile. **e)** Photograph of the prepared stack before collapsing. **f)** Cross-sectional optical microscope image of the cane obtained from the collapsing of the stack (contrast was artificially tuned to highlight the structure).

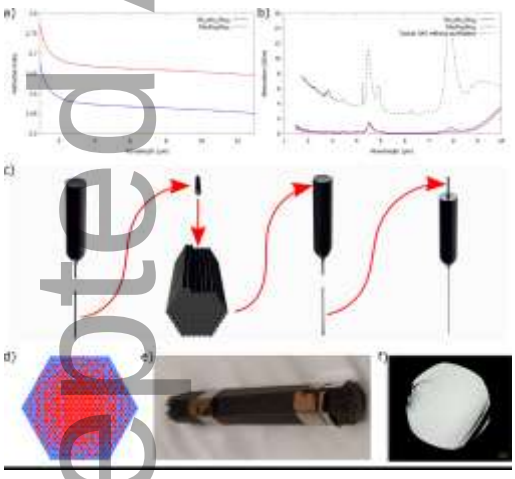

Figure 2: **a),b),c)** Cross-sectional optical microscope image of the fibers with core diameter of 40, 20 and 10 μm respectively (contrast was artificially tuned to highlight the structure). **d)** EDS measurement of the composition across the diameter of the fiber with core size of 40 μm ; the dashed line shows the expected refractive index profile of the fiber. **e)** Attenuation spectrum of the fiber with core diameter of 10 μm , measured in the near-infrared using an optical spectrum analyzer and in the mid-infrared by FTIR spectroscopy. **f)** Near infrared attenuation spectra of the fibers with core diameter $\leq 10\mu$m .

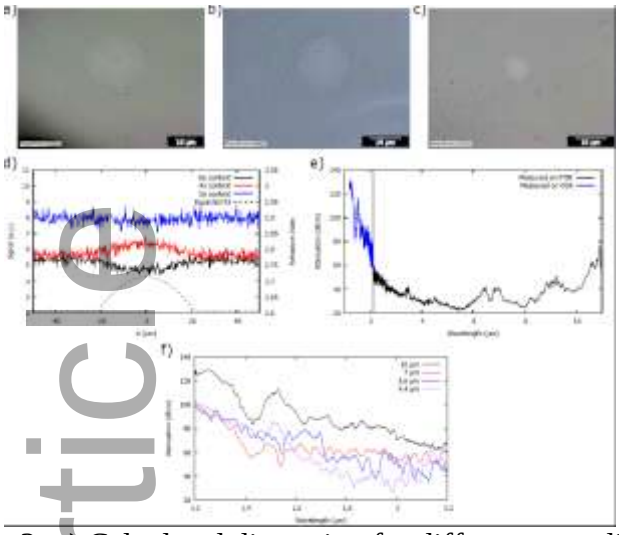

Figure 3: **a)** Calculated dispersion for different core diameters of the chalcogenide GRIN fiber. **b)** Comparison between calculated and measured dispersion for the fiber with a core diameter of 10 μm ; the presented mid-IR curve has been obtained as the average of 8 distinct measurements. **c)** Supercontinuum spectra generated by pumping fibers with different core diameters. **d)** Spectral broadening dynamics with increasing pump power in the fiber with core diameter of 7 μm . **e)** Near field image of light confined in the fiber with core diameter of 7 μm .

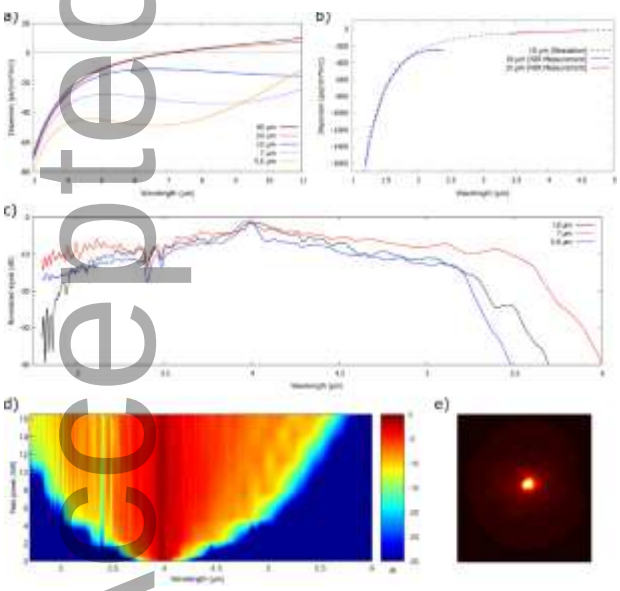

Summary
In this work, high purity chalcogenide glasses in the Ge-As-Se glass system, synthesized in-house, were used for stacking and drawing chalcogenide nanostructured GRIN fibers designed using the Maxwell-Garnett effective medium theory, simulated annealing and genetic algorithms. Generation of a supercontinuum spanning the mid-infrared from 3 µm to 6 µm, pumping at a central wavelength of 4 µm is also reported.